COMMUNICATION

A Ferric Guest Inside a Spin Crossover Ferrous Helicate

Leoní A. Barrios,[a,b] Rosa Diego,[a,b] Mohanad Darawsheh,[a] J. I. Martínez,[c,d] Oliver Roubeau,*[,c,d] and Guillem Aromí*[,a,b]

Received 00th January 20xx,

Accepted 00th January 20xx

DOI: 10.1039/x0xx00000x

A designed dimetallic Fe(II) helicate made with biphenylene-bridged bispyrazolylpyridine ligands and exhibiting a process of spin crossover at temperatures above ambient is shown to encapsulate an *S* = 5/2 tris-oxalato Fe(III) ion. The spin relaxation dynamics of this guest are strongly reduced upon encapsulation.

A major research goal in molecular materials science is the preparation of nanoscale species with tailored functional properties to be implemented as components of spintronic devices.[1, 2] In this context, molecular properties of interest are single-molecule magnet (SMM) behaviour,[3-5] spin crossover (SCO) ability,[6, 7] spin-based quantum bit (qubit) attributes,[8, 9] or photoluminescence.[10, 11] Multitasking molecular entities incorporate more than one such capabilities simultaneously offering the potential of exploiting the synergy between them for specific applications. Efforts in this area have furnished for example, luminescent SMMs,[12, 13] photochromic SCO molecules,[14] SMM guests held by SCO hosts[15] or photo-switchable SMMs.[16, 17] The combination of coordination and supramolecular chemistry offers unlimited possibilities for the design of such composite molecular objects. We have recently designed the synthesis of ferrous $[Fe_2L1_3]^{4+}$ supramolecular helicates where L1 comprises two pyrazolylpyridine (pzpy) fragments linked by a phenylene group.[18, 19] The ability of these fragments to engender SCO on Fe(II)[20, 21] provides an entry for the resulting helicates to this switchable property. In addition, the assembly exhibits a cavity able to host either a Cl^- or a Br^- guest as a means of tuning the SCO properties of the host in the solid state and in solution. A strategy to incorporate larger guests is to engineer the geometry of the ligands to favour the formation of larger cages.[22] Here, we use a longer spacer (biphenyl instead of phenylene) with ligand L (3,3'-bis(3-(pyridin-2-yl)-1H-pyrazol-5-yl)-1,1'-biphenyl Scheme 1) in order to reach SCO $[Fe_2(L)_3]^{4+}$ helicates with a larger cavity. This was capitalized recently to generate an assembly with formula $[Cr(ox)_3]@[Fe_2(L)_3](BF_4)$ (**3**) consisting of a chromic tris-oxalate moiety encapsulated within the corresponding ferrous SCO helicate with the remarkable advantage of inducing for the first time SMM behaviour to a Cr(III) mononuclear entity.[15] This shows an avenue to incorporate other functional guests to the SCO cage, and exploit the possible synergy between both parts of the assembly. Using this strategy, we present here the incorporation of a ferric $[Fe(ox)_3]^{3-}$ unit into the Fe(II) helicate. The free Fe(III) tris-oxalate species has been studied as qubit for quantum computing, yielding quite remarkable quantum coherence properties.[23]

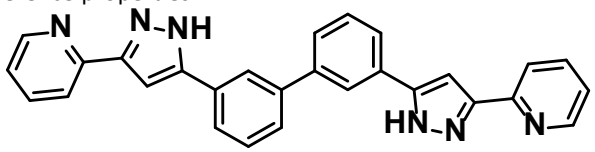

Scheme 1. Ligand L (3,3'-bis(3-(pyridin-2-yl)-1H-pyrazol-5-yl)-1,1'-biphenyl).

The reaction of $Fe(BF_4)_2{\cdot}6H_2O$ with L in MeOH/MeCN in the presence of ascorbic acid (see SI) produced a homogeneous phase of single crystals of the supramolecular coordination salt $[Fe(ox)_3]@[Fe_2L_3](BF_4)$ (**1**). The formation of **1** follows the aerial oxidation of both, a part of the Fe(II) and the ascorbic acid thus

[a] *Departament de Química Inorgànica i Orgànica, Secció Química Inorgànica, Universitat de Barcelona, Barcelona, Spain.*
[b] *Institute of Nanoscience and Nanotechnology of the University of Barcelona (IN2UB), Barcelona, Spain.*
[c] *Instituto de Nanociencia y Materiales de Aragón (INMA), CSIC-Universidad de Zaragoza, Zaragoza, Spain.*
[d] *Departamento de Física de la Material Condensada, Universidad de Zaragoza, Zaragoza, Spain*

† Electronic Supplementary Information (ESI) available: synthetic and analytical details, crystallographic details, views of H-bonding networks, additional magnetic and calorimetric data. See DOI: 10.1039/x0xx00000x

leading to the formation of a guest perfectly suited to sit inside the cavity of an $[Fe_2L_3]^{4+}$ helicate (see below). The original purpose of the ascorbic acid presence was to prevent the oxidation of Fe(II), however, the drive for oxidation and self-assembly led to a completely different result. In this manner, compound **1** consists of a triple stranded $[Fe_2L_3]^{4+}$ helicate encapsulating a ferric $[Fe(ox)_3]^{3-}$ (ox^- = oxalate) complex anion (Fig. 1 and S1), with a BF_4^- anion ensuring the electro-neutrality. The system is found at 100 K in the triclinic space group *P*−1. The unit cell contains two asymmetric units, each of which being composed by one full moiety of **1** together with three molecules of H_2O, in addition to partially occupied and diffuse H_2O and MeOH molecules (see SI).

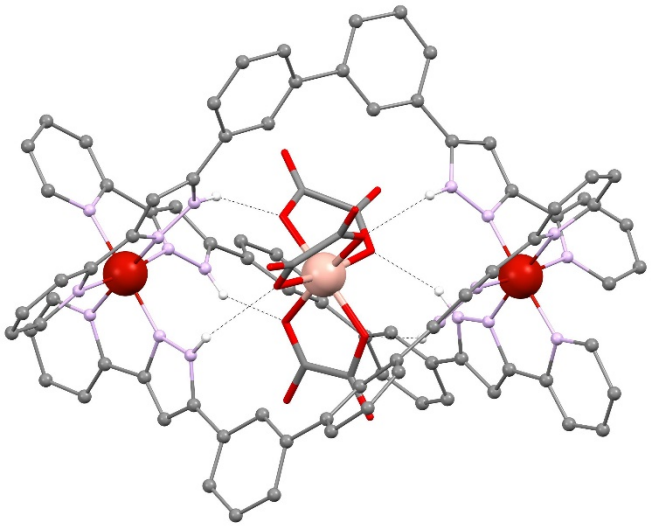

Figure 1. Representation of the supramolecular assembly $([Fe(ox)_3]@[Fe_2L_3])^+$ of **1**. Large red balls are Fe(II), the salmon ball is Fe(III), remaining red is O, grey is C, purple is N and white is H (only hydrogen from N–H groups shown). Dashed lines are H-bonds.

The helicate is formed *via* chelation of each Fe(II) center by pzpy moieties from three L ligands that bind a second metal in the same fashion at the other end. The helicity induced by the pseudo-octahedral geometry around the Fe(II) centres at both ends of the structure, is propagated by the ligands mainly through the rotation around three C–C bonds per ligand; the central bond of the biphenyl and the bonds between the latter and the pzpy groups.‡ The torsion angles around these bonds are finely tuned to fix the central $[Fe(ox)_3]^{3-}$ into the helicate's cavity by means of six O···H–N hydrogen bonds (Table S2). These are formed between the six oxygen atoms coordinated to Fe(III) and the six pyrazolyl N–H groups of the L ligands. Both components of the assembly are chiral and the two enantiomers are present in the unit cell forming a racemic lattice. Within the assembly, the Fe(II)···Fe(III) distances are 5.365 and 5.319 Å, while the inter-ferrous separation is 10.684 Å. At 100 K the average Fe1/2–N bond distances are 1.98/1.97 Å, consistent with the Fe(II) centers lying in the low spin (LS) state at this temperature, as confirmed by the magnetic measurements (see below). The three pairs of oxalate oxygen atoms from the $[Fe(ox)_3]^{3-}$ unit that are not coordinated point away of the assembly through the three large windows opened by the $[Fe_2L_3]^{4+}$ host. In fact, each guest is connected in the lattice to three equivalent guests through these windows by means of hydrogen bonds with molecules of H_2O, acting as bridges. Each of these three guest-guest interactions occurs through one oxygen atom per oxalate ligand, linked to a pair of bridging water molecules. These interactions lead to a two dimensional network of $[Fe(ox)_3]^{3-}$ complexes, each surrounded by its respective host (Fig S2). The stability of the assembly in solution was established by mass spectrometry experiments (Figs. S5-S6, see below).

The process of SCO potentially occurring in **1** above ambient temperature was first examined through its magnetic properties. The χT *vs.* *T* plot (Fig. S7) shows a χT value of 5.13 cm^3Kmol^{-1} at 300 K that declines slightly upon cooling to reach a plateau with a small linear decrease from 5.00 at 260 K to 4.73 at 20 K, thus close to the expected spin-only value of a high-spin (HS) Fe(III) center (*S* = 5/2; 4.375 cm^3Kmol^{-1}). A further decline occurs at the lowest temperatures, down to 4.44 cm^3Kmol^{-1} at 2 K. This thermal response is reproduced upon warming, with χT increasing further and reaching 6.31 cm^3Kmol^{-1} at 400 K. A new cooling cycle (Fig. 2) causes a decrease less pronounced of χT, which reaches a plateau at a temperature similar to that seen in the first cycle. A novel full cycle of warming and cooling leads to χT *vs.* *T* traces that superimpose to that of the just described cooling branch.

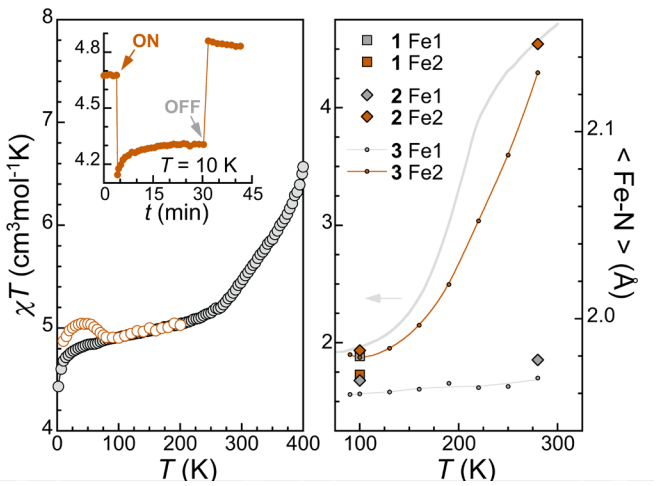

Figure 2. Left: temperature dependence of χT (empty symbols) observed for **1** after an initial warming ramp to 400 K (grey circles). Empty brown circles depict the behaviour after irradiation with green light at 10 K. Inset; variation of χT with time upon turning on and off the 500-600 nm lamp, at *T* = 10 K (jumps are due to local changes in temperature upon switching light on/off). Right: average Fe-N bond lengths at both Fe sites of compounds **1**, **2** and **3**, revealing a SCO process at Fe2 site below 300 K only in **2** and **3**. The full grey line recalls the χT *vs.* *T* plot for **3**.[15]

These data indicate that from 2 K to near 280 K, the Fe(II) centers of the host are in the low-spin (LS) state (*i.e.* *S* = 0), consistent with the structural parameters determined for **1** at 100 by SCXRD (see above). In this range, the system exhibits the Curie-like behaviour expected from the Fe(III) *S* = 5/2 center of the guest, subject to Temperature Independent Paramagnetism (TIP) and zero field splitting (ZFS) effects, the latter evident at very low temperature.

This is consistent with isothermal *M* *vs.* *H* measurements at 2 K, which follow the Brillouin function for *S*= 5/2 spin with *g* =

2.165 (Fig. S8). Above *ca.* 280 K, a gradual transition to the HS of some of the Fe(II) centers becomes evident in the χT *vs.* T plot, although it remains largely incomplete at 400 K. The slightly different path delineated by χT upon cooling is attributed to the desorption of solvent occurred during the warming process, which likely changes slightly the SCO parameters.[18] The latter remain unaltered in the following thermal cycles.

The above results were corroborated by DSC data. A first warming from ambient temperature shows a very energetic and broad peak up to *ca.* 400 K that can be ascribed to solvent loss, in agreement with a weight loss of *ca.* 8 %. A weak shoulder at *ca.* 380 K might correspond to the contribution from the partial SCO (Fig. S9 left), but this remains hypothetical. Subsequent thermal cycles give virtually identical and reproducible DSC traces with a similar very broad hump in the range 250-400 K detected in both cooling and heating ramps, consistent with the SCO process detected in magnetic measurements (Fig 2 left and Fig. S9 right). The associated excess enthalpy $\Delta_{SCO}H$ of *ca.* 17.2 kJmol^{-1}, although relatively large for such a gradual SCO, is reasonable given the temperature range of the SCO process.[24] The excess entropy $\Delta_{SCO}S$ is of the order of 56 Jmol^{-1}K^{-1}, and could correspond to the SCO of one of the two Fe(II) centers. In fact, the temperature dependence of $\Delta H(T)/\Delta_{SCO}H$, which can be considered as depicting the HS fraction throughout the SCO process, shows a reasonable agreement with the magnetic data (Fig. S10). Altogether, magnetic and DSC data give a confident picture agreeing with a gradual SCO at one of the two Fe(II) sites in the range 250-400 K.

Comparing with the thermal SCO observed at *ca.* 200 K for one of the two Fe(II) sites in the Cr(III) analogue (**3**), the assembly reported here reveals a shift of the SCO to higher temperatures, by over 100 K. Such a strong modification of the properties is surprising considering that the oxalate-pyrazole hydrogen bonds are not significantly affected on going from Cr(III) to Fe(III) (Table S2). However, the packing can also have drastic effects and both compounds show a noticeable difference in the hydrogen bonding network involving the $[Fe(ox)_3]^{3-}$ moieties and lattice water molecules (Figs. S2 and S11A), in addition to stronger hydrogen bonds in the case of **1**, with D···A distances about 0.3-0.4 Å shorter.‡ Interestingly, a monoclinic polymorph of **1** can be obtained in different conditions (**2**·3MeOH·4.75H_2O see SI), crystallizing with a unit cell similar to that of **3** and exhibiting a different lattice organization, also reminiscent of that of **3** (Fig. S11B). Variable temperature SCXRD has been valuable in investigating the thermal history of the spin of Fe(II) in molecular materials,[25] and SCXRD of **2** shows average Fe–N bond distances of 1.96 and 1.97 Å at 100 K, while at 280 K these are 1.96 and 2.14 Å, showing that in the monoclinic polymorph **2** one Fe(II) does experience a SCO to the HS state (Fig S12), in the same manner as observed for **3**. This supports the hypothesis that the shift to higher temperatures of the SCO in **1** is largely due to differences in the topology and strength of the $[M(ox)_3]^{3-}$ hydrogen bonding network, and not to the nature of M.

Compound **1** was irradiated at 10 K with light of 500 to 600 nm. An increase of χT, persistent after switching off the irradiation (inset in Fig. 2 left) indicated the occurrence of a phenomenon of light-induced excited spin state trapping (LIESST) that remained, however very inefficient (10% of one Fe site at best). The irradiation is less effective on a polycrystalline powder than a thin pellet (Fig. S15), indicating that the light absorption by the sample and the associated lack of penetration are the main limiting factors. Increasing the temperature causes the relaxation back to the ground LS state, with a characteristic T(LIESST) near 60 K (Fig. 2).

While the purity of **1** was corroborated by microanalysis (SI), the stability in solution of the supramolecular assembly within this compound was studied by positive ion electro spray ionization mass spectrometry (ESI$^+$-MS). The MS experiment was performed in DMSO/acetonitrile and, besides free ligand, the two main peaks observed correspond to the $[Fe(ox)_3]@[Fe_2L_3]^+$ ensemble, probing its persistence in this medium.

This stability solution allowed CW- and TD-EPR frozen solution experiments, which were conducted at X band on a 0.25 mM of **1** in fully deuterated DMSO:MeOH:EtOH (1:36:4). The CW-EPR spectrum obtained at 10 K is consistent with an S = 5/2 Fe(III) HS centre, and can be described by using a Spin Hamiltonian including a Zeeman term and a Zero Field Splitting (ZFS) one with significant rhombicity (Fig. 3 right):[26]

$$H = \mu_B B \cdot g \cdot S + D\left[S_z^2 - S(S+1)\right] + E\left(S_x^2 - S_y^2\right)$$

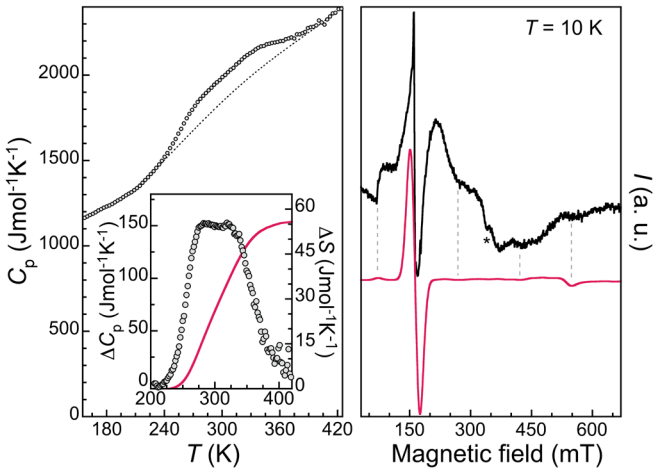

Figure 3. Left: molar heat capacity of **1** (cooling ramp), with the estimated lattice component shown as a dashed line. The inset depicts the derived excess heat capacity (circles) and entropy variation (solid red line) associated to the SCO. Right: frozen solution X-band CW-EPR of **1** at 10 K, together with the simulated spectrum for S = 5/2, D = 0.12 cm^{-1}, E = 0.0335 cm^{-1} and line width of 20 mT, obtained using Easyspin.[27] Vertical dashed grey lines indicate the qualitative agreement for weaker spectral features.

Spectral features displayed at different positions between 70 mT and 600 mT, dominated by the main feature at *ca.* 150 mT (g_{eff} = 4.3) are indication of a ZFS, D, parameter just slightly lower than Zeeman energy. In these conditions, intensities and shapes of the spectral features are largely dependent on details of the spin centre environment, and quantitative simulations are usually not possible. Nevertheless, the main

features of the spectrum are qualitatively reproduced considering D = 0.12 cm^{-1} and E = 0.0335 cm^{-1} (rhombicity parameter E/D = 0.28). The spectrum is similar to those measured for several salts of $[Fe(ox)_3]^{3-}$ and $[Fe(mal)_3]^{3-}$ both in the solid state or in aqueous frozen solution, with comparable Spin Hamiltonian values.[26] Surprisingly, we were unable to detect any electron spin-echo, even at lower temperatures (6 K), while conditions are similar to those used in a previous study of the quantum coherence of free $[Fe(ox)_3]^{3-}$.[23] An estimation of the spin-lattice relaxation time T_1 of **1** in the solid-state was obtained through ac susceptibility measurements, giving *ca.* 20 μs at 2 K and 5000 G (Fig S16). This is more than twice faster than for the $[Cr(ox)_3]^{3-}$ ion in solid **3** at the same field and temperature,[15] but in line with the T_1 of *ca.* 56 μs derived by pulsed EPR on a frozen solution of free $[Fe(ox)_3]^{3-}$ at 7 K.[28] Therefore the absence of spin echo in **1** is probably due to a very short T_2 (*i.e.* below the experimental window, typically < 100 ns), rather than to an exceedingly fast spin relaxation. Considering the T_2 of 1-2 μs reported for frozen solutions of free $[Fe(ox)_3]^{3-}$ in the range 3-7 K,[23, 28] it appears that encapsulation provides more efficient decoherence paths for the guest Fe(III) S = 5/2 spin, possibly resulting from the hydrogen bonding of oxalate oxygens with pyrazole N-H groups of the helicate, thus effectively switching OFF the qubit quantum coherence.

Overall this work shows the ability of dimetallic Fe(II) SCO helicate to encapsulate magnetically active species, thereby affecting their spin relaxation dynamics. The demonstrated light-induced population of metastable Fe(II) HS centers, albeit partial, may also serve to affect the encapsulated qubit.

This research was supported by Spanish MINECO (PGC2018-098630-B-I00, MAT2017-86826-R), the Aragón government (E31_20R PLATON) and the EU (FET-OPEN grant 862893 FATMOLS), and used resources of the ALBA synchrotron and of the Advanced Light Source, which is a DOE Office of Science User Facility under contract no. DEAC02-05CH11231. G. A. thanks the Generalitat de Catalunya for the prize ICREA Academia 2018.

Conflicts of interest

There are no conflicts to declare.

Notes and references

‡ The torsion angles of the phenyl-phenyl and phenyl-pzpy bonds range 35.83 to 41.25° and 7.38 to 25.15°, respectively. Donor-acceptor $O_{water}\cdots O_{ox}$ distances at 100 K range respectively 2.402-2.648 in **1** and 2.779-3.073/2.755-3.014 in **2**/**3**.

1. L. Bogani and W. Wernsdorfer, *Nat. Mater.* 2008, **7**, 179-186.
2. A. S. Zyazin, J. W. G. Van Den Berg, E. A. Osorio, H. S. J. Van Der Zant, N. P. Konstantinidis, M. Leijnse, M. R. Wegewijs, F. May, W. Hofstetter, C. Danieli and A. Cornia, *Nano Lett.* 2010, **10**, 3307-3311.
3. G. A. Craig and M. Murrie, *Chem. Soc. Rev.* 2015, **44**, 2135-2147.
4. D. N. Woodruff, R. E. P. Winpenny and R. A. Layfield, *Chem. Rev.* 2013, **113**, 5110-5148.
5. G. Aromí and E. K. Brechin, *Struct. Bonding (Berlin)* 2006, **122**, 1-67.
6. P. Gütlich, A. B. Gaspar and Y. Garcia, *Beilstein J. Org. Chem.* 2013, **9**, 342-391.
7. G. Kuang, Q. Zhang, T. Lin, R. Pang, X. Shi, H. Xu and N. Lin, *ACS Nano* 2017, **11**, 6295-6300.
8. G. Aromí, D. Aguilà, P. Gamez, F. Luis and O. Roubeau, *Chem. Soc. Rev.* 2012, **41**, 537-546.
9. M. Atzori and R. Sessoli, *J. Am. Chem. Soc.* 2019, **141**, 11339-11352.
10. T. Plakhotnik and V. Palm, *Phys. Rev. Lett.* 2001, **87**.
11. J.-C. G. Bünzli, in *Luminescence of Lanthanide Ions in Coordination Compounds and Nanomaterials*, ed. A. d. Bettencourt-Dias, John Wiley and Sons, Ltd, 2014, ch. 4.
12. J. Wang, J. J. Zakrzewski, M. Heczko, M. Zychowicz, K. Nakagawa, K. Nakabayashi, B. Sieklucka, S. Chorazy and S.-I. Ohkoshi, *J. Am. Chem. Soc.* 2020, **142**, 3970-3979.
13. R. Marin, G. Brunet and M. Murugesu, *Angew. Chem., Int. Ed.* 2021, **60**, 1728-1746.
14. M. Estrader, J. Salinas Uber, L. A. Barrios, J. Garcia, P. Lloyd-Williams, O. Roubeau, S. J. Teat and G. Aromí, *Angew. Chem., Int. Ed.* 2017, **56**, 15622-15627.
15. M. Darawsheh, L. A. Barrios, O. Roubeau, S. J. Teat and G. Aromí, *Angew. Chem., Int. Ed*. 2018, **57**, 13509-13513.
16. A. Fetoh, G. Cosquer, M. Morimoto, M. Irie, O. El-Gammal, G. A. El-Reash, B. K. Breedlove and M. Yamashita, *Sci. Rep*. 2016, **6**, 23785.
17. A. Urtizberea and O. Roubeau, *Chem. Sci.* 2017, **8**, 2290-2295.
18. M. Darawsheh, L. A. Barrios, O. Roubeau, S. J. Teat and G. Aromí, *Chem., Eur. J.* 2016, **22**, 8635-8645.
19. D. Y. Aleshin, R. Diego, L. A. Barrios, Y. V. Nelyubina, G. Aromí and V. V. Novikov, *Angew. Chem., Int. Ed.* 2022, **61**, e202110310.
20. L. S. Harimanow, K. H. Sugiyarto, D. C. Craig, M. L. Scudder and H. A. Goodwin, *Aust. J. Chem.* 1999, **52**, 109.
21. T. Shiga, E. Oshiro, N. Nakayama, K. Mitsumoto, G. N. Newton, H. Nishikawa and H. Oshio, *Eur. J. Inorg. Chem.* 2013, **2013**, 781-787.
22. C. R. K. Glasson, J. K. Clegg, J. C. McMurtrie, G. V. Meehan, L. F. Lindoy, C. A. Motti, B. Moubaraki, K. S. Murray and J. D. Cashion, *Chem. Sci.* 2011, **2**, 540-543.
23. M. J. Graham, J. M. Zadrozny, M. Shiddiq, J. S. Anderson, M. S. Fataftah, S. Hill and D. E. Freedman, *J. Am. Chem. Soc.* 2014, **136**, 7623-7626.
24. O. Roubeau, M. Castro, R. Burriel, J. G. Haasnoot and J. Reedijk, *J. Phys. Chem. B* 2011, **115**, 3003-3012.
25. C. Bartual-Murgui, R. Diego, S. Vela, S. J. Teat, O. Roubeau and G. Aromí, *Inorg. Chem.* 2018, **57**, 11019-11026.
26. D. Collison and A. K. Powell, *Inorg. Chem.* 1990, **29**, 4735-4746.
27. S. Stoll and A. Schweiger, *J. Magn. Reson.* 2006, **178**, 42-55.
28. B. J. Gaffney, G. R. Eaton and S. S. Eaton, *J. Phys. Chem. B* 1998, **102**, 5536-5541.

